AGU PUBLICATIONS

Geophysical Research Letters

RESEARCH LETTER
10.1002/2014GL061100

Key Points:
- We assess neutral sputtering of Phobos by escaping Martian O+ ions
- Martian O+ sputters at rates larger than solar wind depending on SW conditions
- MAVEN may detect the Phobos torus via newly generated torus pickup ions

Correspondence to:
A. R. Poppe,
poppe@ssl.berkeley.edu

Citation:
Poppe, A. R., and S. M. Curry (2014), Martian planetary heavy ion sputtering of Phobos, *Geophys. Res. Lett.*, *41*, doi:10.1002/2014GL061100.

Received 3 JUL 2014
Accepted 27 AUG 2014
Accepted article online 29 AUG 2014

Martian planetary heavy ion sputtering of Phobos

A. R. Poppe[1] and S. M. Curry[1]

[1]Space Sciences Laboratory, University of California, Berkeley, California, USA

Abstract The Martian moons, Phobos and Deimos, have long been suspected to be the sources of tenuous neutral gas tori encircling Mars. While direct outgassing has been ruled out as a strong source, micrometeoroid impact vaporization and charged particle sputtering must operate based on observations at other airless bodies. Previous models have addressed solar wind sputtering of Phobos; however, Phobos and Deimos are also subject to a significant, yet temporally variable, flux of heavy planetary ions escaping from Mars. In this report, we use a combination MHD/test-particle model to calculate the planetary heavy ion flux to Phobos and the ensuing neutral sputtered flux. Depending on ambient solar wind conditions and the location of Phobos, heavy ion sputtering of Phobos generates neutral fluxes up to and exceeding that from solar wind sputtering. We model pickup ions from the Phobos torus itself with applications for observations by the upcoming Mars Atmospheric and Volatile Evolution mission.

1. Introduction

The Martian moons, Phobos and Deimos, have long been postulated as the sources of a pair of tenuous dust and gas tori in orbit around Mars [*Soter*, 1971]. Processes considered as sources of the putative gas tori include micrometeoroid impact vaporization, solar wind charged-particle sputtering, collection and reemission of oxygen from the Martian planetary corona by the putative dust rings, and direct outgassing from the moons themselves [*Fanale and Salvail*, 1989; *Ip and Banaszkiewicz*, 1990; *Sauer et al.*, 1995; *Mura et al.*, 2002; *Cipriani et al.*, 2011]. Much of the motivation for these studies has come from the analysis of observations by the PHOBOS-2 mission of magnetic field and plasma disturbances correlated with the orbital locations of the Martian moons [*Bogdanov*, 1981; *Riedler et al.*, 1989; *Dubinin et al.*, 1990, 1991]. Despite these early observations, later measurements have failed to detect signatures of either dust or gas tori, including optical imaging of the putative ring system [*Duxbury and Ocampo*, 1988; *Showalter et al.*, 2006] or a statistical analysis of magnetic field and electron spectral observations by the Mars Global Surveyor [*Øieroset et al.*, 2010]. Thus, the Phobos and Deimos tori, if they exist at all, must be present at either extremely low densities and/or with significant temporal variability.

Much recent scientific interest has been focused on the long-term evolution of the Martian atmosphere, specifically the potential atmospheric loss processes that have yielded the thin, CO_2-dominated atmosphere seen today [*Jakosky and Phillips*, 2002]. While the overall magnitudes and relative importance of various loss processes is currently under debate, ionization of heavy atmospheric neutrals and subsequent convection away from Mars is known to be one of several ongoing processes [e.g., *Luhmann and Kozyra*, 1991; *Cravens et al.*, 2002; *Carlsson et al.*, 2006; *Fang et al.*, 2008; *Nilsson et al.*, 2011]. Relevant atmospheric ionization processes include photoionization, charge exchange from solar wind protons, and electron impact ionization, each of which is expected to produce distinct distributions and fluxes of escaping atomic and molecular oxygen and carbon dioxide ions [*Curry et al.*, 2013a, 2014]. Depending on the specific plasma and solar conditions and the orientation of the solar wind magnetic and electric fields, models have predicted heavy pickup ion fluxes at a significant fraction of the solar wind proton flux [e.g., *Chaufray et al.*, 2007; *Fang et al.*, 2010; *Curry et al.*, 2014]. Such a large flux of heavy ions may have a significant, if stochastic, effect on the sputtering of neutrals from the surfaces of Phobos and Deimos, as heavy ions are known to sputter neutrals with yields several orders of magnitude greater than that for proton bombardment [*Biersack and Eckstein*, 1984; *Johnson and Baragiola*, 1991; *Behrisch and Eckstein*, 2007]. Studies to date, however, have not previously taken into account the possible role that heavy ions escaping from the Martian atmosphere may play in sputtering significant amounts of neutrals from the surfaces of Phobos and Deimos.

In this paper, we assess the effect of Martian heavy planetary pickup ions on the neutral sputtering rates of Phobos by combining a series of test-particle simulations of escaping Martian atmospheric pickup ions

coupled with neutral sputtering yields from charged-particle impact. We present results specifically for Phobos, noting that qualitatively similar, although smaller in magnitude, results should hold for Deimos. Section 2 describes the pickup ion model and characterizes the predicted fluxes of pickup ions at various locations along the orbit of Phobos while section 3 compares neutral sputtered fluxes resulting from heavy ion bombardment at Phobos with neutrals produced by solar wind sputtering. Finally, section 4 presents pickup ion tracing results for ions from the torus itself and discusses the most favorable conditions for observing Phobos torus pickup ions with the upcoming Mars Atmospheric and Volatile Evolution (MAVEN) mission.

2. Martian Heavy Planetary Ion Fluxes

In order to calculate the flux of heavy planetary ions from the Martian atmosphere to the orbit of Phobos, we use the Mars Test Particle (MTP) model. A detailed description of the model and its results can be found in the literature [*Curry et al.*, 2013a, 2013b], so we only briefly describe the model here. The MTP model is a parallelized, three-dimensional Monte Carlo model that calculates Martian atmospheric and exospheric pickup ion trajectories using background electric and magnetic fields from the multispecies BATS-R-US (Block Adaptive Tree Solar Wind Roe-Type Upwind Scheme) magnetohydrodynamic (MHD) simulations of the Martian magnetosphere [*Ma et al.*, 2004; *Dong et al.*, 2014]. The MHD simulation includes crustal magnetic fields implemented with a 60-degree spherical harmonic scheme from *Arkani-Hamed* [2001] and positioned to face the Sun at 180°W, corresponding to the low-ion outflow case [*Fang et al.*, 2010]. Variations of the ion escape as a function of the position of the Martian crustal fields are addressed in section 3. The solar wind velocity was 400 km/s, and we used two cases for the interplanetary magnetic field: (1) Parker spiral and (2) B_z, both with a strength of 5 nT. The Parker spiral conditions provide a canonical case for comparison, while the B_z interplanetary magnetic field (IMF) case was chosen specifically to investigate the effect of the Martian O^+ plume originating from the oxygen corona [*Brecht and Ledvina*, 2006; *Fang et al.*, 2008, 2010; *Curry et al.*, 2013a] on sputtering at Phobos. For B_z IMF conditions, this plume is in the ecliptic plane and thus will intersect the orbit of Phobos. The MTP traces approximately one billion O^+, O_2^+, and CO_2^+ ions each from the Martian exosphere and oxygen corona (as detailed in *Curry et al.* [2013b]) throughout the simulation domain until they hit the inner or outer boundary. No collisions are taken into account after the creation of each pickup ion, as ion collisional lifetimes are much longer than typical ion transit times through the simulation domain. Virtual detectors in the MTP simulation collect measurements of ion density and velocity distributions at any point, appropriately normalized to calculate the omnidirectional flux. For this study, we placed a series of 30 × 30 km detectors (roughly the cross section of Phobos) along the Phobos orbit at 2.7 R_M to construct velocity space distributions and energy-time spectrograms. For the results presented below, we place the Phobos orbit at a beta-angle of 0° and assume that the solar wind conditions are steady throughout the modeled time. The solar wind and IMF orientation are highly dynamic, and thus, the actual planetary heavy ion flux to Phobos will continuously change as a function of the solar wind and IMF conditions.

Figures 1a and 1b show the MTP model calculations of Martian O^+ flux at Phobos' orbit as a function of local time and energy for two IMF geometries: (a) Parker spiral and (b) B_z/E_y. In the first case, Figure 1a, O^+ fluxes are concentrated almost exclusively in the Martian tail, with energies ranging from 1 eV to 10 keV and fluxes summed over energy on the order of 10^6 cm^{-2} s^{-1}. O^+ pickup ions originating from the outermost tenuous edge of the hot oxygen corona generate low levels of flux ($\approx 10^3 - 10^5$ cm^{-2} s^{-1}) with energies between 1 keV and 10 keV while Phobos is in the magnetosheath and solar wind. In the second case, the IMF is B_z and the convection electric field is E_y, and thus, planetary ions generated in the Martian magnetosheath or out in the solar wind are picked up and accelerated in the plane of Phobos' orbit. Figure 1b shows the O^+ flux for this IMF geometry. Similar to the Parker spiral case, O^+ fluxes are present at a broad range of energies in the Martian magnetotail (21–3 LT), with an additional narrow beam of O^+, typically referred to as the polar plume, from 3 to 8 LT at energies from 1 keV up to nearly 20 keV. Summed over energy, the peak O^+ fluxes for the B_z/E_y case are approximately 10^7 cm^{-2} s^{-1} in the Martian magnetotail and approximately 5×10^6 cm^{-2} s^{-1} in the polar plume. The faint, high-energy (1–10 keV) flux of O^+ ions at Phobos in the magnetosheath and solar wind is also present similar to the Parker spiral case. We also used the MTP to calculate the flux of Martian O_2^+ and CO_2^+ ions to the orbit of Phobos; however, as found in *Curry et al.* [2014], O_2^+ and CO_2^+ fluxes are at least an order of magnitude less than O^+ flux, especially for higher energies and thus do not appreciably contribute to sputtering at Phobos relative to O^+. We note that *Nilsson et al.* [2011] found an

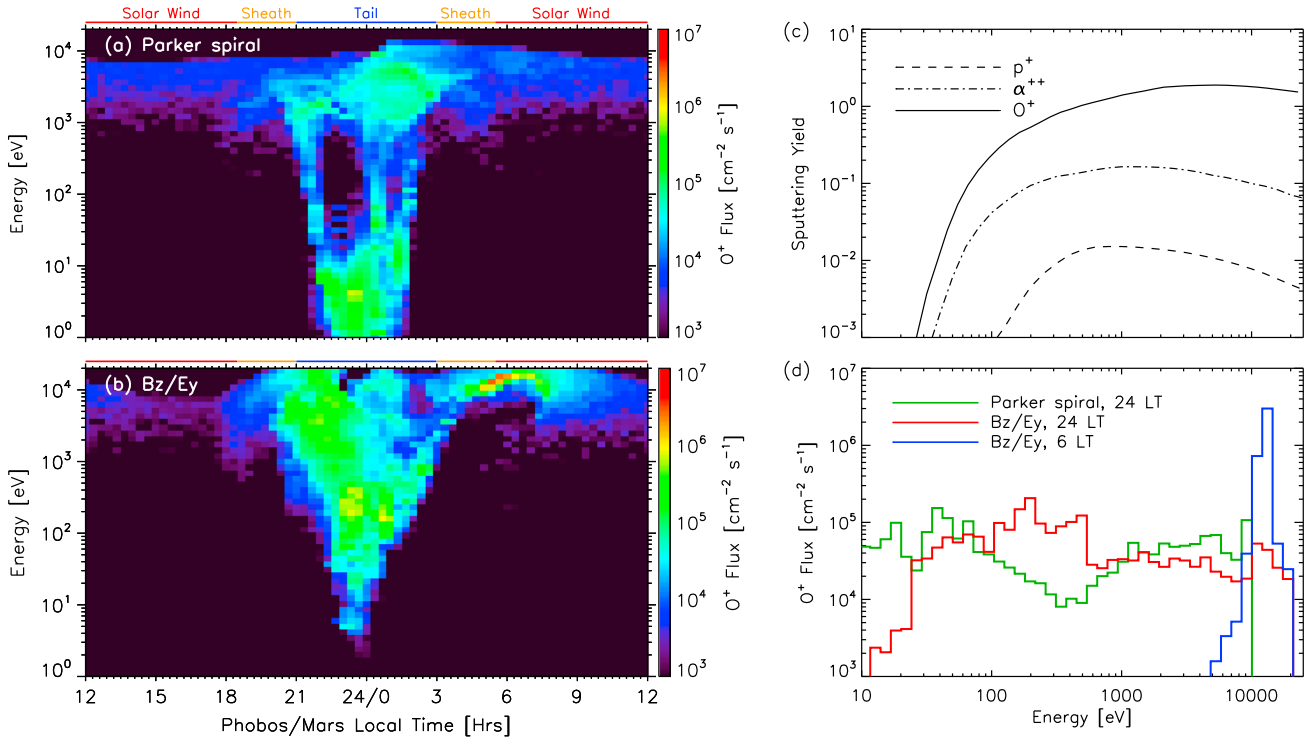

Figure 1. The Martian O^+ flux to Phobos from the MTP model as a function of local time and ion energy for (a) Parker spiral IMF and (b) B_z/E_y IMF, respectively. The approximate Martian magnetospheric region at each time is denoted in color at the top of each panel. (c) The neutral sputtering yields as a function of impacting ion energy for protons (dashed), alphas (dash-dot), and O^+ (solid) [*Biersack and Eckstein*, 1984]. (d) The planetary O^+ flux as a function of energy at selected, specific times for Parker spiral and B_z IMF conditions, as labeled.

O_2^+/O^+ ion escape ratio of 0.66 ± 0.07, larger than that found with the MTP [*Curry et al.*, 2014]; however, this result was based on low-energy (< 50 eV) ions only which do not contribute to sputtering.

3. Sputtered Fluxes From Phobos

Charged-particle sputtering is a fundamental planetary process known to operate throughout the solar system. Energetic charged particles eject neutrals from solid surfaces with yields dependent on the impacting ion's mass, energy, and charge as well as the surface properties. Ion impact angle can also influence yield for polished surfaces; however, for porous or rough surfaces (like that of Phobos) yields have been shown to be independent of impact angle [*Küstner et al.*, 1998]. For our work here, we consider only kinetic sputtering (essentially momentum transfer) [*Biersack and Eckstein*, 1984] and do not include any effects from potential sputtering, relevant only for highly charged ions [*Meyer et al.*, 2011]. The sputtering yields for protons, alphas, and oxygen as a function of energy are shown in Figure 1c. Sputtering yields are a strong function of the impacting ion mass, with peak yields ranging from $\approx 10^{-2}$ for protons to $\approx 10^{-1}$ for alphas ($m = 4$), and > 1 for heavier masses. Additionally, heavier masses have significant yields for a broader range of energies than for protons or alphas, and thus, heavy planetary ions at energies from approximately 50 eV to greater than tens of keV can efficiently sputter neutrals.

For comparison with the neutral sputtering yields, Figure 1d shows the flux of Martian O^+ ions as a function of energy for selected periods for the two IMF conditions presented in Figures 1a and 1b. In green, we show the O^+ energy spectrum at 24 LT for Parker spiral IMF, when Phobos is immersed in the Martian magnetotail ion outflow region. The O^+ energy spectra at this time is particularly broad, with fluxes $> 10^4$ cm^{-2} s^{-1} at energies ranging from 10 eV to nearly 10 keV. Comparison of the O^+ energy spectrum and the heavy ion sputtering yield demonstrates that a large portion of the impacting O^+ flux at Phobos will efficiently sputter neutrals from the surface at yields up to and exceeding unity. Figure 1d also shows the O^+ flux as a function of energy for two discrete local times along Phobos' orbit for B_z/E_y IMF conditions: the spectrum at 24 LT in the Martian magnetotail (red) and at 6 LT (blue) as Phobos crosses the heavy ion polar plume. For these IMF

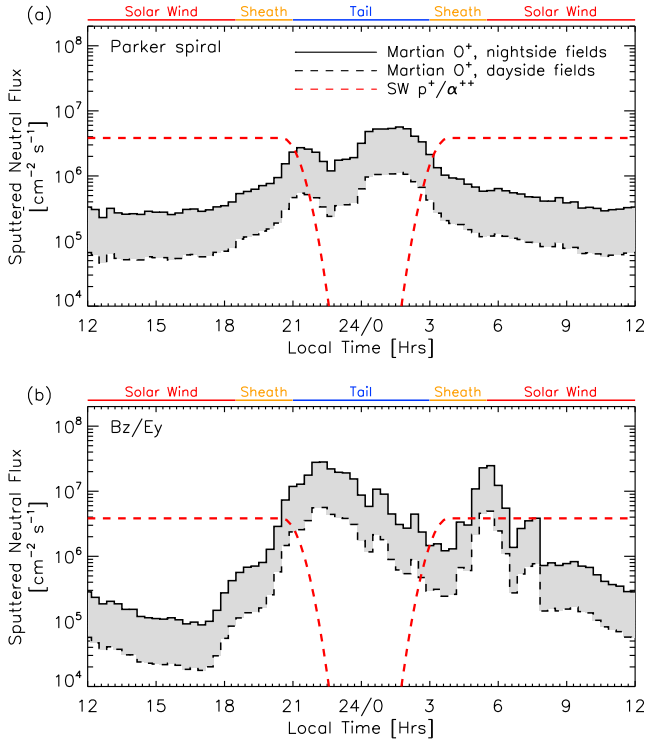

Figure 2. A comparison of the neutral sputtered flux from Phobos induced by solar wind protons and alphas (dashed red lines) and Martian planetary O^+ (solid black lines) for (a) Parker spiral and (b) B_z IMF conditions. The grey-shaded region denotes variability in the O^+ escape flux induced by the varying position of the Martian crustal fields with respect to the subsolar point [*Fang et al.*, 2010].

conditions, the O^+ flux has distinctly different energy distributions at the chosen local times, with the tail outflow fairly broad (similar to the tail outflow spectrum for Parker spiral in green) and the polar plume quite narrow in energy. Nevertheless, the broad sputtering yield as a function of energy for heavy ions implies that planetary O^+ ions are an efficient production mechanism of sputtered neutrals at both times.

The total neutral sputtered flux as a function of position along Phobos' orbit for each case can be calculated by convolving the heavy ion sputtering yields from Figure 1c with the O^+ flux as a function of energy and time shown in Figures 1a and 1b. We have also taken into account the likely porosity of the Phobos regolith, which has been shown to slightly reduce the sputtering yields (a factor of 0.71 relative to a smooth surface) [*Cassidy and Johnson*, 2005]. Figures 2a and 2b show the result of this calculation for Parker spiral and B_z IMF conditions, respectively. Additionally, we have also taken into account the variability in O^+ fluxes as a function of the relative position of the main concentration of Martian crustal fields by plotting a range of sputtered neutral flux. Relative to the dayside crustal field orientation used to generate Figure 1, O^+ fluxes for relevant energies (≈100 eV–1 keV) increase by a factor of 5 for times when the crustal field complex is located on the nightside, as the solar wind penetrates deeper into the Martian exosphere and corona, inducing higher charge exchange and electron impact ionization rates for neutrals [*Fang et al.*, 2010, Table 1]. As expected, the heavy ion sputtering in the Martian magnetotail is present in both conditions, with absolute neutral sputtered fluxes from the surface of Phobos at approximately 8×10^6 cm^{-2} s^{-1} for Parker spiral and approximately 3×10^7 cm^{-2} s^{-1} for B_z IMF. The neutral sputtered flux peaks a second time at 5–6 LT for the B_z IMF case at approximately 3×10^7 cm^{-2} s^{-1} when Phobos crosses the polar plume. As Phobos continues out into the solar wind, heavy ion sputtered fluxes rapidly die off in both cases as the flux of planetary ions correspondingly decreases. For comparison, we also show the typical sputtered neutral flux from the solar wind with a 3% alpha content as the red dashed line at approximately 4×10^6 cm^{-2} s^{-1}, noting that the solar wind sputtered flux ceases during Phobos' transit through the Martian magnetotail. We also note that variations in the solar wind density, speed, and alpha content can induce variability in the sputtered flux by roughly an order of magnitude. Nevertheless, when Phobos' transits through regions of the Martian magnetosphere with significant fluxes of heavy planetary ions, the neutral sputtered flux from Phobos induced by such heavy planetary ions can exceed solar wind sputtered neutral fluxes. This is especially significant when Phobos crosses the magnetotail, where solar wind sputtering ceases, only to be replaced with an equivalent or greater source of sputtered neutrals.

In order to further compare the relative rates of solar wind proton/alpha and Martian planetary heavy ion sputtering, we can compute the orbit-averaged sputtered flux, since both processes are variable along Phobos' orbit. Performing such a calculation yields average sputtered fluxes of 2.3×10^6, $0.2–1.2\times10^6$, and $1.0–4.8\times10^6$ cm^{-2} s^{-1} for solar wind proton/alpha sputtering, heavy ion sputtering with Parker spiral IMF conditions, and heavy ion sputtering with B_z conditions, respectively. Thus, even though planetary heavy

Table 1. The Mass Fraction, Number Fraction, Production Rate, Photoionization Rate, and Peak Pickup Ion Flux for the Dominant Atomic Species Generated Through Sputtering at Phobos

	Fe	Si	O	Mg	Al	Na	Ca
Mass fraction[a,b]	0.21	0.13	0.41	0.10	0.017	0.005	0.001
Number fraction	0.09	0.11	0.64	0.14	0.015	0.005	0.001
Production rate [s^{-1}]	3.2×10^{18}	3.9×10^{18}	2.2×10^{19}	5×10^{18}	5.3×10^{17}	1.8×10^{17}	3.6×10^{16}
Photoionization rate[c], 1.5 AU [s^{-1}]	6.1×10^{-6}	1.6×10^{-5}	2×10^{-7}	4×10^{-7}	5.6×10^{-4}	3.4×10^{-6}	1.4×10^{-4}
Peak torus pickup ion flux [cm^{-2} s^{-1}]	5.7×10^{3}	6.9×10^{3}	4.0×10^{4}	1×10^{4}	0.9×10^{3}	3.1×10^{2}	7×10^{1}

[a] *Vernazza et al.* [2010].
[b] *Cipriani et al.* [2011].
[c] *Huebner et al.* [1992].

ion sputtering operates only during limited portions along Phobos' orbit, it contributes a nearly equal number of neutrals as solar wind sputtering does. As a useful number for further comparisons and modeling exercises, the total neutral loss rate from Phobos due to the combination of solar wind and planetary heavy ion sputtering is approximately 1.5–6 $\times 10^{19}$ s^{-1}, depending on IMF conditions. This rate, despite the increase from planetary heavy ion sputtering, is still quite low compared to early estimates of active outgassing rates from Phobos and Deimos on the order of 10^{23} s^{-1} [*Sauer et al.*, 1995].

4. Phobos Torus Pickup Ions

While previous studies have suggested either imaging of energetic neutral atoms generated from charge-exchange collisions between torus neutrals and solar wind protons [*Mura et al.*, 2002] or imaging of solar scattering from torus neutrals [*Cipriani et al.*, 2011] as methods for detecting the torus, one can also consider the detection of freshly ionized pickup ions from the torus generated through photoionization, charge exchange, or electron impact ionization. Ions from the Phobos torus will respond to the background electric and magnetic fields, similar to Martian planetary ions, and thus, spacecraft with ion mass composition experiments, such as the Suprathermal and Thermal Ion Composition (STATIC) experiment on board MAVEN, may be able to detect and identify these ions. To calculate the absolute magnitude of the torus pickup ion flux, we model the neutral distribution of the torus as azimuthally symmetric, independent of the location of Phobos, with a characteristic cross-sectional radius of 100 km [c.f., *Mura et al.*, 2002]. The assumption of azimuthal symmetry is generally valid for all species as the drift time of a sputtered neutral with respect to Phobos is typically longer than the neutral's ionization lifetime. We use the bulk mass composition of Phobos calculated previously by *Vernazza et al.* [2010] and used by *Cipriani et al.* [2011], listed in Table 1, followed by the equivalent number fraction by species. Using the total sputtered production rate of neutrals from Phobos of approximately 5×10^{19} s^{-1} calculated in section 3, the production rate by individual species is listed in the third row. We note that *Cipriani et al.* [2011] also estimated the neutral production rate from micrometeoroid bombardment and found production rates on the order of 10^{17} s^{-1}; thus, we safely neglect this source of neutrals. The photoionization rate for each species scaled to 1.5 AU for solar median conditions is listed in the third row of Table 1 [*Huebner et al.*, 1992], noting that charge exchange and electron impact ionization may also contribute to the ionization of torus neutrals. Using these ionization rates, we traced test particles through the MHD electric and magnetic fields and calculated the isotropic pickup ion flux as a function of position in near-Mars space. We simulated Al^+ (m = 27 amu) and Fe^+ (m = 56 amu) as representative species and selected B_z IMF conditions, as this ensures a concentration of torus pickup ions in the ecliptic plane. A full study of torus pickup ions under a wide range of IMF/solar wind conditions is beyond the scope of the current work but identified as a future study.

Figure 3 shows the omnidirectional flux of (a) Al^+ and (b) Fe^+ pickup ions generated from the Phobos neutral torus for B_z IMF conditions projected onto the ecliptic plane, each normalized to the maximum flux recorded in the simulation. Ions generated out in the solar wind (roughly 6 to 18 LT) undergo classical pickup trajectories in the ecliptic plane and are convected away from Mars, while noting that some fraction of these pickup ions precipitate down into the atmosphere of Mars similar to ions from the Martian corona [e.g., *Luhmann and Kozyra*, 1991]. Ions born from the torus in the dusk sector of the Martian magnetosheath (18 to 22 LT) transit through the Martian magnetotail. Interestingly, the superposition of these trajectories

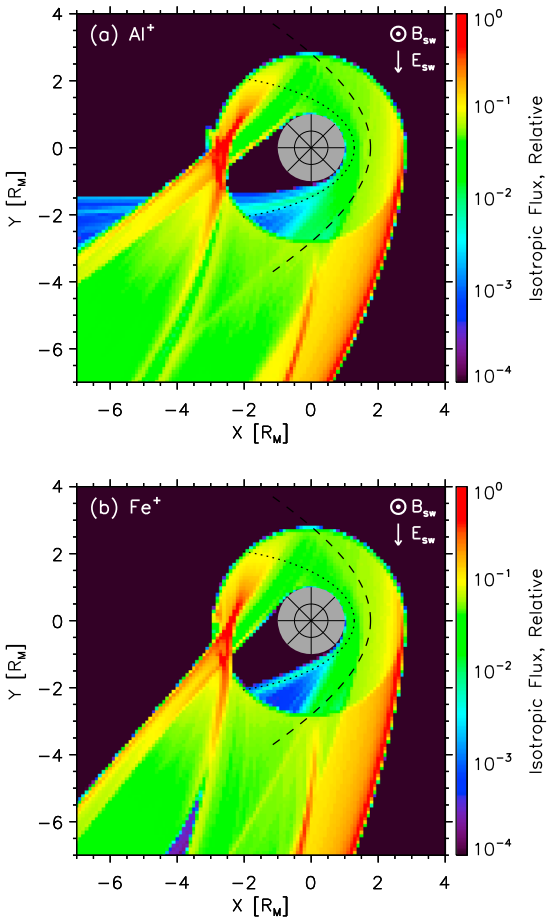

Figure 3. The normalized, isotropic flux of (a) Al^+ and (b) Fe^+ pickup ions from the Phobos neutral torus at $r = 2.7\ R_m$ for B_z IMF conditions, projected onto the ecliptic plane. The dotted and dashed lines show the average magnetic pileup boundary and bow shock locations, respectively [from *Vignes et al.*, 2000]. The solar wind magnetic and electric field vectors are also plotted for reference.

for both Al^+ and Fe^+ converges near midnight in the magnetotail, resulting in an enhancement in the omnidirectional flux similar to that seen along the edge of the escaping pickup ion plume in the solar wind originating from 6 to 12 LT. Other, smaller enhancements in the pickup ion fluxes, such as the linear streak originating from $r = [0.0, -2.7]\ R_M$ and extending downward, are due to the overlapping of pickup ion trajectories originating from locations along the torus with slight variations in the local electric and magnetic fields. Such changes are found at the solar wind/magnetosheath boundary (i.e., the Martian bow shock) and at points within the Martian magnetotail. For B_z IMF conditions, the most favorable locations for observing pickup ions from the Phobos torus are off the dawn sector out in the solar wind ($r > 2.7\ R_m$) or in the Martian magnetotail near local midnight just inside the orbit of Phobos. We list the peak pickup ion flux for each species in the last row of Table 1. The total peak flux over all species at their peak is approximately 10^5 cm^{-2} s^{-1} although nearly half of this flux is from oxygen, which may be difficult to detect against the background O^+ flux from the Martian atmosphere and corona. Nevertheless, given favorable spacecraft position and solar wind/IMF conditions, it may be possible for ion mass composition instruments, such as MAVEN/STATIC which, with sufficient integration times, can detect energy fluxes down to 10^4 eV/cm^2-s-str-eV, to observe Phobos torus pickup ion fluxes near Mars, especially given the anticipated angular anisotropy of the pickup ion beams.

5. Conclusion

We have assessed the impact of escaping planetary O^+ ions from Mars on the surface sputtering of Phobos and the production of the Phobos neutral torus. While solar wind sputtering is a strong source of sputtered neutrals, sputtering by planetary O^+ ions can equal or exceed solar wind sputtering rates depending on IMF conditions and the location of Phobos. Escaping O^+ fluxes are nearly always present in the Martian magnetotail at a wide range of energies and thus serve as a strong source of sputtering while Phobos crosses the magnetotail once every 7.5 h. This flux essentially replaces solar wind sputtering, which ceases during Martian magnetotail crossings. Additionally, depending on the IMF orientation, a plume of high-energy (>10 keV) O^+ ions intersects the orbit of Phobos, leading to additional heavy ion sputtering of Phobos, although such a process is time-variable due to the constantly changing IMF conditions.

We have also performed simulations of the generation of pickup ions generated from the Phobos neutral torus itself and followed these ions through the MHD fields in order to estimate the possibility that these ions can be observed with in situ plasma instrumentation. While the typical fluxes of Phobos torus pickup ions are quite low, the convergence of pickup ion trajectories from continuous regions of the Phobos torus yields specific positions within the magnetosphere of Mars where the pickup ion flux is concentrated. These convergences depend on both the external IMF conditions and the dynamic structure of the Martian magnetosheath and tail yet nevertheless present the best possibility for detection via pickup ion observations.

The MAVEN mission, due to arrive at Mars in September 2014, will have a nominal apoapsis just inside the orbit of Phobos and thus, based on our calculations presented here, may be able to remotely detect the neutral Phobos torus via pickup ions.

Acknowledgments

A.R.P. gratefully acknowledges support from NASA's Solar System Exploration Research Virtual Institute (SSERVI). This publication is SSERVI contribution SSERVI-2014-171. A.R.P. also acknowledges the International Space Science Institute (ISSI) for hosting a workshop series that in part inspired this work. S.M.C. acknowledges support from the Mars Atmosphere and Volatile Evolution (MAVEN) mission. The authors thank C. Dong for providing MHD simulation results. The authors also thank F. Cipriani and two other reviewers for constructive comments. Data used in this analysis are available from the authors upon request.

The Editor thanks three anonymous reviewers for their assistance in evaluating this paper.

References

Arkani-Hamed, J. (2001), A 50-degree spherical harmonic model of the magnetic field of Mars, *J. Geophys. Res.*, *106*(E10), 23,197-23,208.

Behrisch, R., and W. Eckstein (2007), *Sputtering by Particle Bombardment: Experiments and Computer Calculations From Threshold to MeV Energies*, Topics in Applied Physics, vol. 110, Springer, Berlin, Heidelberg, New York.

Biersack, J. P., and W. Eckstein (1984), Sputtering studies with the Monte Carlo Program TRIM.SP, *Appl. Phys. A*, *34*, 73–94.

Bogdanov, A. V. (1981), Mars satellite Deimos interactions with the solar wind and its influence on flow around Mars, *J. Geophys. Res.*, *86*(A8), 6926–6932.

Brecht, S. H., and S. A. Ledvina (2006), The solar wind interaction with the Martian ionosphere/atmosphere, *Space Sci. Rev.*, *124*(1–4), 164–173.

Carlsson, E., et al. (2006), Mass composition of the escaping plasma at Mars, *Icarus*, *182*, 320–328.

Cassidy, T. A., and R. E. Johnson (2005), Monte Carlo model of sputtering and other ejection processes within a regolith, *Icarus*, *176*, 499–507.

Chaufray, J. Y., R. Modolo, F. Leblanc, G. Chanteur, R. E. Johnson, and J. G. Luhmann (2007), Mars solar wind interaction: Formation of the Martian corona and atmospheric loss to space, *J. Geophys. Res.*, *112*, E09009, doi:10.1029/2007JE002915.

Cipriani, F., O. Witasse, F. Leblanc, R. Modolo, and R. E. Johnson (2011), A model of interaction of Phobos' surface with the Martian environment, *Icarus*, *212*, 643–648.

Cravens, T. E., A. Hoppe, and S. A. Ledvina (2002), Pickup ions near Mars associated with escaping oxygen atoms, *J. Geophys. Res.*, *107*(A8), 1170–1180, doi:10.1029/2001JA000125.

Curry, S. M., M. Liemohn, X. Fang, Y. Ma, and J. Espley (2013a), The influence of production mechanisms on pick-up ion loss at Mars, *J. Geophys. Res. Space Physics*, *118*, 554–569, doi:10.1029/2012JA017665.

Curry, S. M., M. Liemohn, X. Fang, D. Brain, and Y. Ma (2013b), Simulated kinetic effects of the corona and solar cycle on high altitude ion transport at Mars, *J. Geophys. Res. Space Physics*, *118*, 3700–3711, doi:10.1002/jgra.50358.

Curry, S. M., M. Liemohn, X. Fang, Y. Ma, J. Slavin, J. Espley, S. Bougher, and C. F. Dong (2014), Test particle comparison of heavy atomic and molecular ion distributions at Mars, *J. Geophys. Res. Space Physics*, *119*, 2328–2344, doi:10.1002/2013JA019221.

Dong, C., S. Bougher, Y. Ma, G. Toth, A. Nagy, and D. Najib (2014), Solar wind interaction with Mars upper atmosphere: Results from the one-way coupling between the multi-fluid MHD model and the MTGCM model, *Geophys. Res. Lett.*, *41*, 2708–2715, doi:10.1002/2014GL059515.

Dubinin, E., R. Lundin, N. F. Pissarenko, S. V. Barabash, A. V. Zakharov, H. Koskinen, K. Schwingenshuh, and Y. G. Yeroshenko (1990), Indirect evidences for a gas/dust torus along the Phobos orbit, *Geophys. Res. Lett.*, *17*(6), 861–864.

Dubinin, E. M., N. F. Pissarenko, S. V. Barabash, A. V. Zakharov, R. Lundin, R. Pellinen, and K. Schwingenschuh (1991), Plasma and magnetic field effects associated with Phobos and Deimos tori, *Planet. Space Sci.*, *39*(1–2), 113–121.

Duxbury, T. C., and A. C. Ocampo (1988), Mars—Satellite and ring search from Viking, *Icarus*, *76*, 160–162.

Fanale, F. P., and J. R. Salvail (1989), Loss of water from Phobos, *Geophys. Res. Lett.*, *16*(4), 287–290.

Fang, X., M. W. Liemohn, A. F. Nagy, Y. Ma, D. L. De Zeeuw, J. U. Kozyra, and T. H. Zurbuchen (2008), Pickup oxygen ion velocity space and spatial distribution around Mars, *J. Geophys. Res.*, *113*, A02210, doi:10.1029/2007JA012736.

Fang, X., M. W. Liemohn, A. F. Nagy, J. G. Luhmann, and Y. Ma (2010), On the effect of the Martian crustal magnetic field on atmospheric erosion, *Icarus*, *206*, 130–138.

Huebner, W. F., J. J. Keady, and S. P. Lyon (1992), Solar photo rates for planetary atmospheres and atmospheric pollutants, *Astrophys. Space Sci.*, *195*, 1–294.

Ip, W.-H., and M. Banaszkiewicz (1990), On the dust/gas tori of Phobos and Deimos, *Geophys. Res. Lett.*, *17*(6), 857–860.

Jakosky, B. M., and R. J. Phillips (2002), Mars volatile and climate history, *Nature*, *412*, 237–244.

Johnson, R. E., and R. Baragiola (1991), Lunar surface: Sputtering and secondary ion mass spectrometry, *Geophys. Res. Lett.*, *18*(11), 2169–2172.

Küstner, M., W. Eckstein, V. Dose, and J. Roth (1998), The influence of surface roughness on the angular dependence of the sputtering yield, *Nucl. Instrum. Methods Phys. Res., Sect. B*, *145*(3), 320–331.

Luhmann, J. G., and J. U. Kozyra (1991), Dayside pickup oxygen ion precipitation at Venus and Mars: Spatial distributions, energy deposition and consequences, *J. Geophys. Res.*, *96*(A4), 5457–5467.

Ma, Y., A. Nagy, I. V. Sokolov, and K. C. Hansen (2004), Three-dimensional, multispecies, high spatial resolution MHD studies of the solar wind interaction with Mars, *J. Geophys. Res.*, *109*, A07211, doi:10.1029/2003JA010367.

Meyer, F. W., P. R. Harris, C. N. Taylor, H. M. Meyer III, A. F. Barghouty, and J. H. Adams (2011), Sputtering of lunar regolith simulant by protons and singly and multicharged Ar ions at solar wind energies, *Nucl. Instrum. Methods Phys. Res., Sect. B*, *269*, 1316–1320.

Mura, A., A. Milillo, S. Orsini, E. Kallio, and S. Barabash (2002), Energetic neutral atoms at Mars: 2. Imaging of the solar wind-Phobos interaction, *J. Geophys. Res.*, *107*(A10), 1278, doi:10.1029/2001JA000328.

Nilsson, H., N. J. T. Edberg, G. Stenberg, S. Barabash, M. Holmström, Y. Futaana, R. Lundin, and A. Fedorov (2011), Heavy ion escape from Mars, influence from solar wind conditions and crustal magnetic fields, *Icarus*, *215*, 475–484.

Øieroset, M., D. A. Brain, E. Simpson, D. L. Mitchell, T. D. Phan, J. S. Halekas, R. P. Lin, and M. H. Acuña (2010), Search for Phobos and Deimos gas/dust tori using in situ observations from Mars global surveyor MAG/ER, *Icarus*, *206*, 189–198.

Riedler, W., et al. (1989), Magnetic fields near Mars: First results, *Nature*, *341*, 604–607.

Sauer, K., E. Dubinin, K. Baumgärtel, and A. Bogdanov (1995), Deimos: An obstacle to the solar wind, *Science*, *269*(5227), 1075–1078.

Showalter, M. R., D. P. Hamilton, and P. D. Nicholson (2006), A deep search for Martian dust rings and inner moons using the Hubble Space Telescope, *Planet. Space Sci.*, *54*, 844–854.

Soter, S. (1971), The dust belts of Mars, *CRSR Rep. 462*, Center for Radiophysics and Space Research (CRSR), Cornell Univ., Ithaca, N. Y.

Vernazza, P., et al. (2010), Meteorite analogs for Phobos and Deimos: Unraveling the origin of the Martian moons, *Meteorit. Planet. Sci. Suppl.*, *73*, 5076.

Vignes, D., C. Mazelle, H. Rme, M. Acuña, J. E. P. Connerney, R. P. Lin, D. L. Mitchell, P. Cloutier, D. H. Crider, and N. F. Ness (2000), The solar wind interaction with Mars: Locations and shapes of the bow shock and the magnetic pile-up boundary from the observations of the MAG/ER experiment onboard Mars global surveyor, *Geophys. Res. Lett.*, *27*(1), 49–52.